Multi-Stage Modeling of Turbine Engine Rotor Vibration

Sang Heon Song, Matthew Castanier, Christophe Pierre

▶ **To cite this version:**

Sang Heon Song, Matthew Castanier, Christophe Pierre. Multi-Stage Modeling of Turbine Engine Rotor Vibration. ASME 2005 International Design Engineering Technical Conferences and Computers and Information in Engineering Conference, Sep 2005, Long Beach, United States. pp.1533-1543, ⟨10.1115/DETC2005-85740⟩. ⟨hal-04629445⟩

HAL Id: hal-04629445

https://hal.science/hal-04629445v1

Submitted on 4 Jul 2024

HAL is a multi-disciplinary open access archive for the deposit and dissemination of scientific research documents, whether they are published or not. The documents may come from teaching and research institutions in France or abroad, or from public or private research centers.

L'archive ouverte pluridisciplinaire **HAL**, est destinée au dépôt et à la diffusion de documents scientifiques de niveau recherche, publiés ou non, émanant des établissements d'enseignement et de recherche français ou étrangers, des laboratoires publics ou privés.

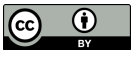

Distributed under a Creative Commons CC BY 4.0 - Attribution - International License

Proceedings of IDETC/CIE 2005
ASME 2005 International Design Engineering Technical Conferences
& Computers and Information in Engineering Conference
September 24-28, 2005, Long Beach, California USA

DETC2005-85740

MULTI-STAGE MODELING OF TURBINE ENGINE ROTOR VIBRATION

Sang Heon Song
Graduate Student Research Assistant
Email: shsong@umich.edu

Matthew P. Castanier *
Associate Research Scientist
Email: mpc@umich.edu

Christophe Pierre
Stephen P. Timoshenko Collegiate Professor
Email: pierre@umich.edu

Department of Mechanical Engineering
The University of Michigan
Ann Arbor, MI 48109-2125, USA

ABSTRACT

In this study, an efficient approach for modeling the vibration of multi-stage rotors is proposed in order to allow more realistic predictions of the free and forced response of bladed disks. The reduced-order modeling approach is based on component mode synthesis, with each stage (bladed disk) treated as a separate component. Thus, each component retains cyclic symmetry, and single-sector models may be used for calculating the component modes. Because adjacent stages typically have different numbers of blades, the single-stage models are synthesized by projecting the stage-to-stage interface motion onto a common basis of circumferentially harmonic shapes. In this manner, any mismatch between sector sizes and finite element meshes at the interface can be handled systematically and automatically, without requiring additional multi-point constraints. For further size reduction, secondary modal analysis is performed on the entire synthesized model. Therefore, only a small set of multi-stage modes are retained in the final reduced-order model, yielding an extremely compact model that retains high accuracy relative to the parent finite element model.

1 INTRODUCTION

There has been a large amount of research devoted to understanding and predicting the vibration response of bladed disks. Early studies generally employed lumped parameter models. [1–5] More recently, finite element models of bladed disks have been used to generate reduced-order models via component mode synthesis methods [6–11] or other reduction techniques [12, 13]. Most of this previous work has been limited to modeling individual bladed disks, even though a bladed disk is typically one stage of a multi-stage rotor. However, Bladh et al. [14] showed that connecting a second stage to a single-stage finite element model of a bladed disk can lead to significant changes for predictions of the maximum blade amplitudes. The discrepancies between single- and multi-stage predictions were especially large when considering the important effects of random discrepancies among blades, or mistuning, on the vibration response. For some mistuning cases, dramatic changes in the first stage's sensitivity to mistuning were observed. This was explained by the fact that presence of the second stage alters blade-to-blade coupling through the disk for the first stage, which is a critical factor for mistuning sensitivity. It was also found that applying constraints to the boundary degrees of freedom of a single stage could not faithfully capture the boundary conditions of the actual stage-to-stage connection. Furthermore, multi-stage rotors exhibit certain types of modes and response patterns that are extended across multiple stages, which are not captured by current single-stage models. Therefore, it is believed that multi-stage

*Address all correspondence to this author.

modeling is essential to improving the predictive capabilities of mistuned bladed disk simulations.

However, modeling multi-stage rotors poses some daunting computational challenges. A key challenge is that the coupling among multiple stages destroys the cyclic symmetry of the system, because each stage has a different number of blades. This means that even idealized, tuned models of the multi-stage assembly would incur prohibitively high computational costs when using traditional finite element analysis, because all sectors of all stages would need to be modeled.

In this work, an efficient approach to multi-stage vibration modeling is developed by adopting a component-based reduced-order modeling approach, which requires only single-sector finite element models of the individual stages. In particular, a component mode synthesis [15–17] approach is employed, with each stage being a component. [18] The stage-to-stage boundaries are thus the interfaces between components. The component modes for each stage are calculated for the tuned case, using cyclic symmetry routines for a single-sector finite element model of each stage. The multi-stage model is assembled by taking advantage of axisymmetry of the stage-to-stage interface surface: the interface motion of each stage is projected onto a common basis of shapes that are harmonic in the circumferential direction. This makes it possible to enforce displacement compatibility at the interface without applying multi-point constraints, despite the mismatch of sector sizes and finite element meshes at the interface. Furthermore, secondary modal analysis is employed [8] to reduce the size of the multi-stage system model. Because there are many degrees of freedom at the stage-to-stage interfaces, the size of the component mode synthesis model may still be too large for efficient predictions of multi-stage response. Therefore, a modal analysis is performed on this model, yielding modes of the full multi-stage assembly, which may then be truncated to obtain a compact reduced-order model for the frequency range of interest.

This paper is organized as follows. In the second section, an example multi-stage finite element model is considered. The finite element model has a realistic geometry, but the size is kept small enough to allow finite element analysis of the full multi-stage model. A simplified multi-stage finite element model is also constructed by eliminating the blades on all but one of the stages, which yields a model that has cyclic symmetry and enables the use of the same vibration analysis techniques used for individual bladed disks. It is shown that predictions from a single-stage model and the simplified multi-stage model do not match the true multi-stage forced response results in a frequency range of interest. In the third section, the new multi-stage reduced-order modeling method is presented. In the fourth section, the proposed modeling method is examined and validated using a two-stage finite element model. Conclusions are drawn and summarized in the final section.

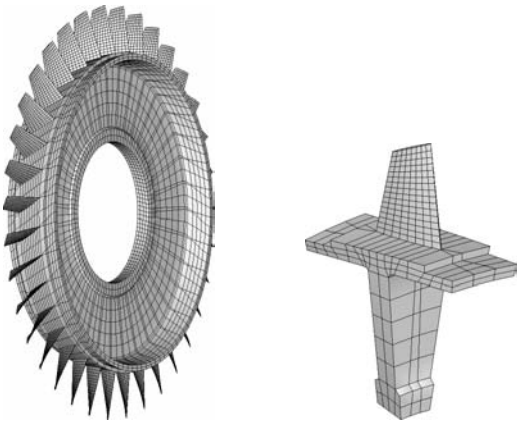

(a) FULL BLADED DISK (b) ONE SECTOR

Figure 1. SINGLE-STAGE FINITE ELEMENT MODEL

2 SINGLE- AND MULTI-STAGE FINITE ELEMENT MODELS

To motivate this study, consider the finite element model (FEM) of a single turbine engine rotor stage, or bladed disk, shown in Fig. 1(a). For the nominal design in which all blades are identical, a bladed disk has cyclic symmetry. Therefore, the FEM of only one sector, as shown in Fig. 1(b), can be used to calculate the response of the full bladed disk. This provides great computational savings. In reality, there are always discrepancies among the blades, or mistuning, and this can have a drastic effect on the bladed disk vibration. However, state-of-the-art modeling techniques for mistuned bladed disks still employ tuned sector models and cyclic symmetry analysis in the reduced-order modeling procedure [11–13]. Given that an industrial FEM of a full bladed disk may have millions of degrees of freedom (DOF), it is important to be able to take advantage of cyclic symmetry as much as possible to reduce computational costs.

It is important to note, however, that a bladed disk is typically one stage of a multi-stage rotor. An example of a three-stage rotor is shown in Fig. 2, which includes the bladed disk of Fig. 1 as the second stage. For a multi-stage rotor, each stage has a different number of blades, and therefore even the ideal or "tuned" system does not possess cyclic symmetry. This implies that all sectors of all stages need to be included in a multi-stage vibration model, which clearly poses tremendous numerical challenges. As a result, vibration modeling and analysis methods to date have generally been developed for individual bladed disks with some assumed boundary conditions applied at the stage-to-stage connections. For example, a vibration analysis for the second stage of the three-stage model shown in Fig. 2 might be performed using the single-stage model shown in Fig. 1 with the boundary DOF held fixed in the axial direction.

In order to reduce the effects of the applied boundary condi-

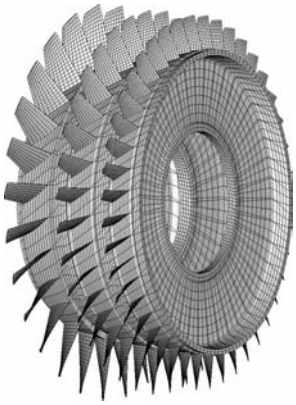

Figure 2. THREE-STAGE FINITE ELEMENT MODEL

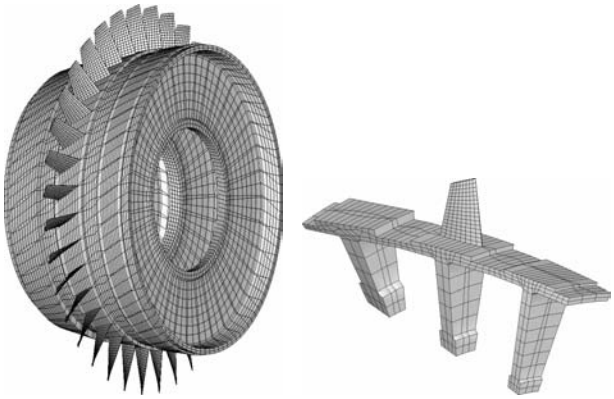

(a) FULL MODEL (b) SECTOR MODEL

Figure 3. CENTER-STAGE FINITE ELEMENT MODEL

tions, an alternative finite element modeling approach would be to include the disks of the adjacent stages. An example is shown in Fig. 3(a), which consists of the bladed disk of Fig. 1(a) with adjacent disks attached. Of course, this is also the three-stage model of Fig. 2 with the blades removed from stages 1 and 3. Because this model is intended to simulate the vibration response of the center stage of a three-stage section, here it is referred to as a center-stage model. The advantage of this center-stage approach is that the model retains cyclic symmetry (assuming that the sectors with neglected blades have axisymmetric disks, which is not the case if the disks have slots for inserted blades, bolts at spacers, etc.). This allows tuned free and forced response analysis to be performed using standard cyclic symmetry routines available in finite element analysis software. Fig. 3(b) shows one sector of the center-stage model. Note that, for all practical purposes, the center-stage model is really just a bladed disk with a complex disk section, which means that any vibration modeling or analysis method developed for bladed disks may be employed for the center-stage model. The question, however, is whether vibration predictions based on a single-stage or center-stage model can accurately match those from a multi-stage model.

Figure 4 shows forced response results for stage 2 using three different tuned system models: the single-stage FEM of Fig. 1, the center-stage FEM of Fig. 3, and the three-stage FEM of Fig. 2. For each model, engine order 4 excitation was applied at a single node on each blade tip for stage 2 only. As can be seen, significant differences exist between the results from the single- and three-stage models. This is in agreement with the results shown by Bladh et al. [14] for a simpler example system. Furthermore, even the results from the center-stage model do not match those of the three-stage model. This indicates that neglecting the blades on adjacent stages—and, consequently, neglecting the stage-to-stage periodicity mismatch—can have a significant effect on the multi-stage vibration predictions. More importantly, it suggests that a more comprehensive multi-stage modeling approach needs to be developed. This is addressed in the next section.

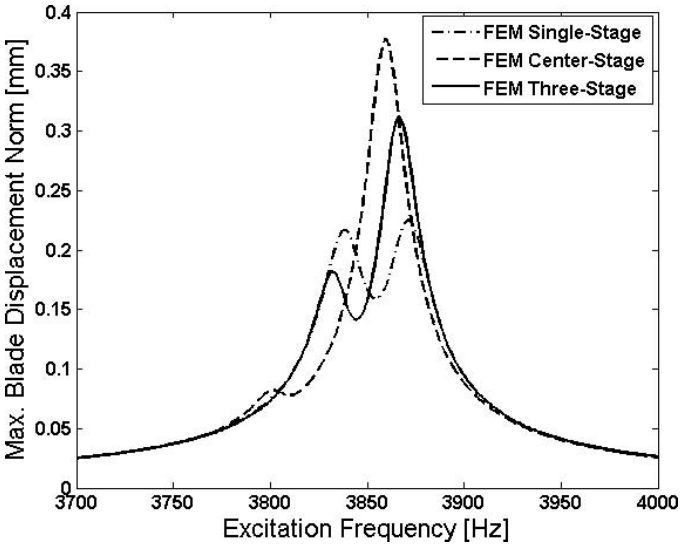

Figure 4. FORCED RESPONSE RESULTS FOR SINGLE-, CENTER-, AND THREE-STAGE MODELS

3 REDUCED-ORDER MODELING WITH STAGE-BY-STAGE COMPONENT MODE SYNTHESIS

In this section, a reduced-order vibration modeling method is presented for multi-stage turbine engine rotors. The technique is based on component mode synthesis (CMS), with each stage treated as a separate component. This allows component mode calculations to be performed with only a sector FEM for each stage and enables the use of cyclic symmetry analysis routines. Synthesis of the stages is achieved through a coordinate transfor-

mation of the constraint modes for each stage to a set of shapes that feature displacement compatibility for both stages at the stage-to-stage interface. This allows a CMS model to be built without requiring that the finite element meshes match on adjacent stages or having to manually apply multi-point constraints. A modal analysis is then performed on the CMS model to retrieve mode shapes for the multi-stage system, which provides a compact basis for simulating the vibration of the multi-stage rotor. This modeling process is described in more detail in the following subsections.

3.1 Individual Components with Cyclic Symmetry

As the basic framework for the multi-stage modeling approach, the Craig-Bampton component mode synthesis method [16] is used, with each stage treated as a separate component. In the Craig-Bampton method, the component motion is represented by two sets of modes: (1) component normal modes—the vibration modes of the component with the interface DOF held fixed; and (2) constraint modes—the static shapes induced by enforcing a unit displacement at each interface DOF in turn, with all other interface DOF held fixed. Therefore, the first step in the multi-stage modeling method is to calculate the component normal modes and the constraint modes for each stage.

For the i_{th} stage, the motion of all degrees of freedom can be described by those of one sector FEM using cyclic symmetry analysis. Therefore, the physical coordinates and corresponding mass and stiffness matrices of a i_{th} stage can be expressed as:

$$\boldsymbol{x}^i = \begin{Bmatrix} \tilde{\boldsymbol{x}}^i_\sigma \\ \tilde{\boldsymbol{x}}^i_s \\ \tilde{\boldsymbol{x}}^i_\tau \end{Bmatrix} \tag{1a}$$

$$\boldsymbol{M}^i = \begin{bmatrix} \tilde{\boldsymbol{M}}^i_{\sigma\sigma} & \tilde{\boldsymbol{M}}^i_{\sigma s} & \tilde{\boldsymbol{M}}^i_{\sigma\tau} \\ & \tilde{\boldsymbol{M}}^i_{ss} & \tilde{\boldsymbol{M}}^i_{s\tau} \\ Sym. & & \tilde{\boldsymbol{M}}^i_{\tau\tau} \end{bmatrix}, \boldsymbol{K}^i = \begin{bmatrix} \tilde{\boldsymbol{K}}^i_{\sigma\sigma} & \tilde{\boldsymbol{K}}^i_{\sigma s} & \tilde{\boldsymbol{K}}^i_{\sigma\tau} \\ & \tilde{\boldsymbol{K}}^i_{ss} & \tilde{\boldsymbol{K}}^i_{s\tau} \\ Sym. & & \tilde{\boldsymbol{K}}^i_{\tau\tau} \end{bmatrix}, \tag{1b}$$

where

$$\tilde{\boldsymbol{x}}^i_* = \begin{Bmatrix} \vdots \\ \boldsymbol{x}^h_* \\ \vdots \end{Bmatrix}^i_{h=0,\ldots,H^i}, H^i = \begin{cases} \frac{N^i}{2} & \text{if } N^i \text{ is even} \\ \frac{N^i-1}{2} & \text{if } N^i \text{ is odd} \end{cases}.$$

$$\tilde{\boldsymbol{M}}^i_{**} = \underset{h=0,\ldots,H^i}{\tilde{\mathbf{B}}\mathbf{diag}} \left[\boldsymbol{M}^h_{**}\right]^i$$

$$\tilde{\boldsymbol{K}}^i_{**} = \underset{h=0,\ldots,H^i}{\tilde{\mathbf{B}}\mathbf{diag}} \left[\boldsymbol{K}^h_{**}\right]^i$$

In the above, h is the harmonic number, N^i is the number of blades for stage i, σ denotes the interface DOF to the upstream stage, s denotes the interior DOF, τ denotes the interface DOF to the downstream stage, and $\underset{h=0,\ldots,H^i}{\tilde{\mathbf{B}}\mathbf{diag}} \left[*\right]^i$ denotes a pseudo-block-diagonal matrix for the i_{th} stage.

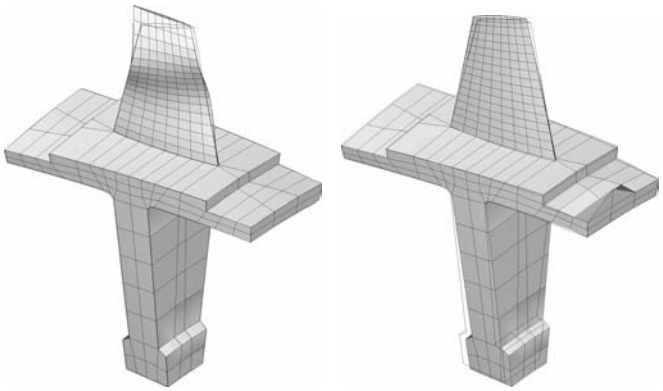

(a) NORMAL MODE (b) CONSTRAINT MODE

Figure 5. COMPONENT MODES CALCULATED WITH A SECTOR MODEL

Also using cyclic symmetry properties, the single-sector FEM can be used to calculate the component normal modes ($\tilde{\boldsymbol{\Phi}}^i$) and the static constraint modes at the interface with both upstream ($\tilde{\boldsymbol{\Psi}}^i_\sigma$) and downstream ($\tilde{\boldsymbol{\Psi}}^i_\tau$) stages. These modal matrices have the form:

$$\tilde{\boldsymbol{\Phi}}^i = \underset{h=0,\ldots,H^i}{\tilde{\mathbf{B}}\mathbf{diag}} \left[\boldsymbol{\Phi}^h\right]^i \tag{2a}$$

$$\tilde{\boldsymbol{\Psi}}^i_\sigma = \underset{h=0,\ldots,H^i}{\tilde{\mathbf{B}}\mathbf{diag}} \left[\boldsymbol{\Psi}^h_\sigma\right]^i \tag{2b}$$

$$\tilde{\boldsymbol{\Psi}}^i_\tau = \underset{h=0,\ldots,H^i}{\tilde{\mathbf{B}}\mathbf{diag}} \left[\boldsymbol{\Psi}^h_\tau\right]^i \tag{2c}$$

Typical component modes are shown in Fig. 5 for the single-sector model.

With these component normal modes and static constraint modes, the physical coordinates of i_{th} stage can be transformed to a mixed basis of modal coordinates and physical interface coordinates:

$$\begin{Bmatrix} \tilde{\boldsymbol{x}}^i_\sigma \\ \tilde{\boldsymbol{x}}^i_s \\ \tilde{\boldsymbol{x}}^i_\tau \end{Bmatrix} = \begin{bmatrix} \boldsymbol{I} & \boldsymbol{0} & \boldsymbol{0} \\ \tilde{\boldsymbol{\Psi}}^i_\sigma & \tilde{\boldsymbol{\Phi}}^i & \tilde{\boldsymbol{\Psi}}^i_\tau \\ \boldsymbol{0} & \boldsymbol{0} & \boldsymbol{I} \end{bmatrix} \begin{Bmatrix} \tilde{\boldsymbol{x}}^i_\sigma \\ \tilde{\boldsymbol{q}}^i_\Phi \\ \tilde{\boldsymbol{x}}^i_\tau \end{Bmatrix}, \tag{3}$$

where $\tilde{\boldsymbol{q}}^i_\Phi$ denotes modal coordinates corresponding to the kept component normal modes, $\tilde{\boldsymbol{\Phi}}^i$. With this transformation, the mass and stiffness matrices of the i_{th} stage can be projected to

the mixed coordinates $\boldsymbol{q}^i$.

$$\boldsymbol{q}^i = \begin{Bmatrix} \tilde{\boldsymbol{x}}^i_\sigma \\ \tilde{\boldsymbol{q}}^i_\Phi \\ \tilde{\boldsymbol{x}}^i_\tau \end{Bmatrix} \tag{4a}$$

$$\boldsymbol{\mu}^i = \begin{bmatrix} \tilde{\boldsymbol{\mu}}^i_{\sigma\sigma} & \tilde{\boldsymbol{\mu}}^i_{\sigma\Phi} & \tilde{\boldsymbol{\mu}}^i_{\sigma\tau} \\ & \boldsymbol{I} & \tilde{\boldsymbol{\mu}}^i_{\Phi\tau} \\ Sym. & & \tilde{\boldsymbol{\mu}}^i_{\tau\tau} \end{bmatrix}, \boldsymbol{\kappa}^i = \begin{bmatrix} \tilde{\boldsymbol{\kappa}}^i_{\sigma\sigma} & \boldsymbol{0} & \tilde{\boldsymbol{\kappa}}^i_{\sigma\tau} \\ & \tilde{\boldsymbol{\Lambda}}^i & \boldsymbol{0} \\ Sym. & & \tilde{\boldsymbol{\kappa}}^i_{\tau\tau} \end{bmatrix}, \tag{4b}$$

where

$$\begin{aligned}
\tilde{\boldsymbol{\mu}}^i_{\sigma\sigma} &= {\tilde{\boldsymbol{\Psi}}^i_\sigma}^T \tilde{\boldsymbol{M}}^i_{ss} \tilde{\boldsymbol{\Psi}}^i_\sigma + {\tilde{\boldsymbol{\Psi}}^i_\sigma}^T \tilde{\boldsymbol{M}}^i_{s\sigma} + \tilde{\boldsymbol{M}}^i_{\sigma s} \tilde{\boldsymbol{\Psi}}^i_\sigma + \tilde{\boldsymbol{M}}^i_{\sigma\sigma} \\
\tilde{\boldsymbol{\mu}}^i_{\sigma\Phi} &= {\tilde{\boldsymbol{\Psi}}^i_\sigma}^T \tilde{\boldsymbol{M}}^i_{ss} \tilde{\boldsymbol{\Phi}}^i + \tilde{\boldsymbol{M}}^i_{\sigma s} \tilde{\boldsymbol{\Phi}}^i \\
\tilde{\boldsymbol{\mu}}^i_{\sigma\tau} &= {\tilde{\boldsymbol{\Psi}}^i_\sigma}^T \tilde{\boldsymbol{M}}^i_{ss} \tilde{\boldsymbol{\Psi}}^i_\tau + {\tilde{\boldsymbol{\Psi}}^i_\sigma}^T \tilde{\boldsymbol{M}}^i_{s\tau} + \tilde{\boldsymbol{M}}^i_{\sigma s} \tilde{\boldsymbol{\Psi}}^i_\tau + \tilde{\boldsymbol{M}}^i_{\sigma\tau} \\
\tilde{\boldsymbol{\mu}}^i_{\Phi\tau} &= {\tilde{\boldsymbol{\Phi}}^i}^T \tilde{\boldsymbol{M}}^i_{ss} \tilde{\boldsymbol{\Psi}}^i_\tau + {\tilde{\boldsymbol{\Phi}}^i}^T \tilde{\boldsymbol{M}}^i_{s\tau} \\
\tilde{\boldsymbol{\mu}}^i_{\tau\tau} &= {\tilde{\boldsymbol{\Psi}}^i_\tau}^T \tilde{\boldsymbol{M}}^i_{ss} \tilde{\boldsymbol{\Psi}}^i_\tau + {\tilde{\boldsymbol{\Psi}}^i_\tau}^T \tilde{\boldsymbol{M}}^i_{s\tau} + \tilde{\boldsymbol{M}}^i_{\tau s} \tilde{\boldsymbol{\Psi}}^i_\tau + \tilde{\boldsymbol{M}}^i_{\tau\tau} \\
\tilde{\boldsymbol{\kappa}}^i_{\sigma\sigma} &= {\tilde{\boldsymbol{\Psi}}^i_\sigma}^T \tilde{\boldsymbol{K}}^i_{ss} \tilde{\boldsymbol{\Psi}}^i_\sigma + {\tilde{\boldsymbol{\Psi}}^i_\sigma}^T \tilde{\boldsymbol{K}}^i_{s\sigma} + \tilde{\boldsymbol{K}}^i_{\sigma s} \tilde{\boldsymbol{\Psi}}^i_\sigma + \tilde{\boldsymbol{K}}^i_{\sigma\sigma} \\
\tilde{\boldsymbol{\kappa}}^i_{\sigma\tau} &= {\tilde{\boldsymbol{\Psi}}^i_\sigma}^T \tilde{\boldsymbol{K}}^i_{ss} \tilde{\boldsymbol{\Psi}}^i_\tau + {\tilde{\boldsymbol{\Psi}}^i_\sigma}^T \tilde{\boldsymbol{K}}^i_{s\tau} + \tilde{\boldsymbol{K}}^i_{\sigma s} \tilde{\boldsymbol{\Psi}}^i_\tau + \tilde{\boldsymbol{K}}^i_{\sigma\tau} \\
\tilde{\boldsymbol{\kappa}}^i_{\tau\tau} &= {\tilde{\boldsymbol{\Psi}}^i_\tau}^T \tilde{\boldsymbol{K}}^i_{ss} \tilde{\boldsymbol{\Psi}}^i_\tau + {\tilde{\boldsymbol{\Psi}}^i_\tau}^T \tilde{\boldsymbol{K}}^i_{s\tau} + \tilde{\boldsymbol{K}}^i_{\tau s} \tilde{\boldsymbol{\Psi}}^i_\tau + \tilde{\boldsymbol{K}}^i_{\tau\tau},
\end{aligned}$$

and $\tilde{\boldsymbol{\Lambda}}^i$ is a diagonal matrix of eigenvalues for the normal modes kept for the i_{th} stage.

3.2 Interface Coordinate Transformation to Fourier Basis Shapes

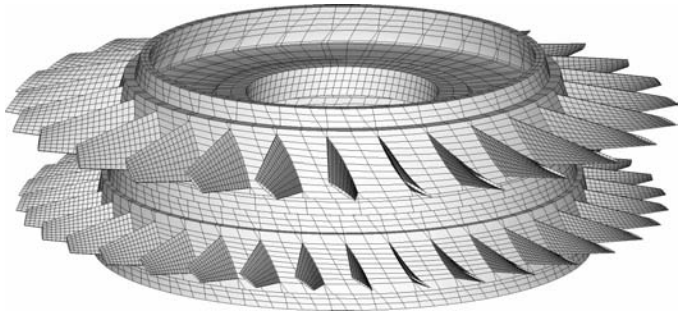

Figure 6. TWO-STAGE FINITE ELEMENT MODEL

To illustrate the problem of synthesizing adjacent stages at their interface, consider the two-stage rotor shown in Fig. 6. These stages have different numbers of blades, and due to this

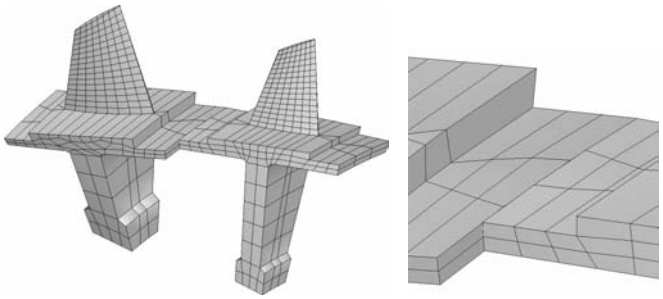

(a) SECTOR SIZE MISMATCH (b) MESH MISMATCH

Figure 7. PERIODICITY AND MESH MISMATCH AT THE INTERFACE

periodicity mismatch between stages the single-sector models do not sweep the same angle in the circumferential direction. Furthermore, stage 1 has 27 blades and stage 2 has 35 blades, which are relative primes, and this is typical of adjacent stages. Therefore, it would take an extremely fine mesh in order to have all of the finite element nodes coincide at the interface between stages. In general, there is a mismatch between the meshes at each stage-to-stage interface. The periodicity and mesh mismatch for this example two-stage FEM is shown in Fig. 7.

Thus, in order to handle the general case, it is assumed here that the coordinates corresponding to the interstage boundaries of the i_{th} and $(i+1)_{th}$ stages at their interface will not match, such that:

$$\tilde{\boldsymbol{x}}^i_\tau \neq \tilde{\boldsymbol{x}}^{i+1}_\sigma, \tag{5}$$

where

$$\tilde{\boldsymbol{x}}^i_\tau = \begin{Bmatrix} \vdots \\ \boldsymbol{x}^h_\tau \\ \vdots \end{Bmatrix}^i_{h=0,\ldots,H^i} \quad , \quad \tilde{\boldsymbol{x}}^{i+1}_\sigma = \begin{Bmatrix} \vdots \\ \boldsymbol{x}^h_\sigma \\ \vdots \end{Bmatrix}^{i+1}_{h=0,\ldots,H^{i+1}}$$

However, it is important to note that the structural connection between stages, called the spacer, is axisymmetric in the region between the disks. Therefore, if the single-stage components are defined by cutting the spacer along a flat surface that is perpendicular to the axis of symmetry, the interstage interface will itself be axisymmetric, having the shape of an annular plate. This makes it natural to use a Fourier series to define a common basis of interface shapes that are purely harmonic in the circumferential direction. Of course, the actual mesh at the interface is discrete, with a different discretization for each stage. However, one needs only to define a common basis for the interface motion and project the constraint modes onto this basis to enforce displacement compatibility. Therefore, by establishing this Fourier

basis, the stages may be synthesized in a systematic and automated manner, obviating the need to manually apply multi-point constraints. The main caveat is that the number of harmonics (number of Fourier basis shapes) that can be used is limited by the coarser of the two meshes in the circumferential direction. This means that the highest harmonics must be neglected for the finer mesh in order to have a one-to-one match of Fourier basis shapes for each stage. However, by definition this means discarding only very short wavelength motion at the interface, which should not pose a problem for solving vibration problems of interest. In fact, in practice these shapes can be truncated further if one wishes to reduce the size of the resultant synthesized model.

Using the approach outlined above, the physical coordinates of the interface ($\boldsymbol{x}_\tau^i$) can be described with new coordinates ($\tilde{\boldsymbol{x}}_\upsilon^i$) composed of a finite number of Fourier basis shapes associated with the physical DOF along one radial line segment in the interface, denoted by $\boldsymbol{x}_\upsilon$:

$$\tilde{\boldsymbol{x}}_\upsilon^i = \left\{ \begin{matrix} \vdots \\ \boldsymbol{x}_\upsilon^h \\ \vdots \end{matrix} \right\}_{h=0,\ldots,H^i}^{i}, H^i = \begin{cases} \frac{\eta_\upsilon^i}{2} & \text{if } \eta_\upsilon^i \text{ is even} \\ \frac{\eta_\upsilon^i - 1}{2} & \text{if } \eta_\upsilon^i \text{ is odd} \end{cases} \tag{6}$$

where η_υ^i is the number of Fourier basis shapes, and the transformation matrix from $\tilde{\boldsymbol{x}}_\upsilon^i$ to $\boldsymbol{x}_\tau^i$ can be defined with $\hat{\boldsymbol{S}}_{\tau\upsilon}^i$:

$$\boldsymbol{x}_\tau^i = \hat{\boldsymbol{S}}_{\tau\upsilon}^i \tilde{\boldsymbol{x}}_\upsilon^i \,, \tag{7}$$

where $\hat{\boldsymbol{S}}_{\tau\upsilon}^i = \boldsymbol{S}_{\eta_\tau^i,\eta_\upsilon^i} \otimes \boldsymbol{I}$, and $\boldsymbol{S}_{\eta_\tau^i,\eta_\upsilon^i}$ is an η_τ^i by η_υ^i extended real-valued Fourier matrix defined by

$$\boldsymbol{S}_{\eta_\tau^i,\eta_\upsilon^i}(j,k) = \begin{cases} \sqrt{\frac{1}{\eta_\upsilon^i}} & \text{if } k = 1 \\ \sqrt{\frac{2}{\eta_\upsilon^i}} \cdot cos\left[(j-1)\frac{2\pi}{\eta_\tau^i}\frac{k}{2}\right] & \text{if } k \text{ is even} \\ \sqrt{\frac{2}{\eta_\upsilon^i}} \cdot sin\left[(j-1)\frac{2\pi}{\eta_\tau^i}\frac{k-1}{2}\right] & \text{if } k \text{ is odd } (\neq 1) \end{cases} .$$

In the above equation, η_τ^i denotes the number of radial segments on the interstage interface (τ) of i_{th} stage, and '$\otimes$' denotes the Kronecker tensor product. Also, non-cyclic physical coordinates of the interface ($\boldsymbol{x}_\tau^i$) can be described with cyclic physical coordinates ($\tilde{\boldsymbol{x}}_\tau^i$).

$$\boldsymbol{x}_\tau^i = \hat{\boldsymbol{F}}^i \tilde{\boldsymbol{x}}_\tau^i \,, \tag{8}$$

where $\hat{\boldsymbol{F}}^i = \boldsymbol{F}_{N^i} \otimes \boldsymbol{I}$, and $\boldsymbol{F}_{N^i}$ denotes a real-valued Fourier matrix ($\boldsymbol{F}_{N^i} = \boldsymbol{S}_{N^i,N^i}$). From Eq. (7) and Eq. (8), the relation between cyclic physical interface coordinates ($\tilde{\boldsymbol{x}}_\tau^i$) and new interface coordinates ($\tilde{\boldsymbol{x}}_\upsilon^i$) can be obtained with a transformation matrix denoted by $\boldsymbol{\Pi}_{\tau\upsilon}^i$:

$$\tilde{\boldsymbol{x}}_\tau^i = \boldsymbol{\Pi}_{\tau\upsilon}^i \tilde{\boldsymbol{x}}_\upsilon^i \,, \tag{9}$$

where $\boldsymbol{\Pi}_{\tau\upsilon}^i = \hat{\boldsymbol{F}}^{i^T} \hat{\boldsymbol{S}}_{\tau\upsilon}^i$. In the same manner, cyclic physical coordinates of the interface to the upstream stage ($\tilde{\boldsymbol{x}}_\sigma^i$) can be related to the corresponding interface coordinates ($\tilde{\boldsymbol{x}}_\xi^i$) with a similar transformation matrix denoted by $\boldsymbol{\Pi}_{\sigma\xi}^i$. By using a common radial line segment ($\boldsymbol{x}_\upsilon^i = \boldsymbol{x}_\xi^{i+1}$) and the same number of Fourier basis shapes ($\eta_\upsilon^i = \eta_\xi^{i+1}$) for the interface of adjacent stages, their interface coordinates can be made kinematically compatible:

$$\tilde{\boldsymbol{x}}_\upsilon^i = \tilde{\boldsymbol{x}}_\xi^{i+1} \tag{10}$$

It should be noted that the assumptions of a common radial line segment and evenly spaced radial segments were made for convenience, to simplify the notation, and are not required.

3.3 Component Synthesis

For simplicity, and without loss of generality, the synthesis procedure is derived for two adjacent stages, the i_{th} and $(i+1)_{th}$ stages. The two-stage system has coordinates $\tilde{\boldsymbol{x}}_\xi^i$, $\tilde{\boldsymbol{q}}_\Phi^i$, $\tilde{\boldsymbol{x}}_\upsilon^i (= \tilde{\boldsymbol{x}}_\xi^{i+1})$, $\tilde{\boldsymbol{q}}_\Phi^{i+1}$, and $\tilde{\boldsymbol{x}}_\upsilon^{i+1}$, which denote interstage interface coordinates between the $(i-1)_{th}$ and i_{th} stages, modal cyclic DOF for the i_{th} stage, interstage interface coordinates between the i_{th} and $(i+1)_{th}$ stages, modal cyclic DOF for the $(i+1)_{th}$ stage, and interstage interface coordinates between the $(i+1)_{th}$ and $(i+2)_{th}$ stages, respectively. The transformation from component coordinates to the two-stage system coordinates can be defined with the transformation matrices, $\boldsymbol{\Pi}_{\sigma\xi}^i$, $\boldsymbol{\Pi}_{\tau\upsilon}^i$, $\boldsymbol{\Pi}_{\sigma\xi}^{i+1}$, and $\boldsymbol{\Pi}_{\tau\upsilon}^{i+1}$ obtained in section 3.2. Using this transformation, the mass and the stiffness matrices for the two-stage system can be synthesized as:

$$\boldsymbol{q}^{syn} = \begin{Bmatrix} \tilde{\boldsymbol{x}}_\xi^i \\ \tilde{\boldsymbol{q}}_\Phi^i \\ \tilde{\boldsymbol{x}}_\upsilon^i (= \tilde{\boldsymbol{x}}_\xi^{i+1}) \\ \tilde{\boldsymbol{q}}_\Phi^{i+1} \\ \tilde{\boldsymbol{x}}_\upsilon^{i+1} \end{Bmatrix} \tag{11a}$$

$$\boldsymbol{\mu}^{syn} = \begin{bmatrix} \boldsymbol{\mu}_{\xi\xi}^i & \boldsymbol{\mu}_{\xi\Phi}^i & \boldsymbol{\mu}_{\xi\upsilon}^i & \boldsymbol{0} & \boldsymbol{0} \\ & \boldsymbol{I} & \boldsymbol{\mu}_{\Phi\upsilon}^i & \boldsymbol{0} & \boldsymbol{0} \\ & & \boldsymbol{\mu}_{\upsilon\upsilon}^i + \boldsymbol{\mu}_{\xi\xi}^{i+1} & \boldsymbol{\mu}_{\xi\Phi}^{i+1} & \boldsymbol{\mu}_{\xi\upsilon}^{i+1} \\ & Sym. & & \boldsymbol{I} & \boldsymbol{\mu}_{\Phi\upsilon}^{i+1} \\ & & & & \boldsymbol{\mu}_{\upsilon\upsilon}^{i+1} \end{bmatrix} \tag{11b}$$

$$\boldsymbol{\kappa}^{syn} = \begin{bmatrix} \boldsymbol{\kappa}^i_{\xi\xi} & \mathbf{0} & \boldsymbol{\kappa}^i_{\xi\upsilon} & \mathbf{0} & \mathbf{0} \\ & \tilde{\boldsymbol{\Lambda}}^i & \mathbf{0} & \mathbf{0} & \mathbf{0} \\ & & \boldsymbol{\kappa}^i_{\upsilon\upsilon} + \boldsymbol{\kappa}^{i+1}_{\xi\xi} & \mathbf{0} & \boldsymbol{\kappa}^{i+1}_{\xi\upsilon} \\ & Sym. & & \tilde{\boldsymbol{\Lambda}}^{i+1} & \mathbf{0} \\ & & & & \boldsymbol{\kappa}^{i+1}_{\upsilon\upsilon} \end{bmatrix} \tag{11c}$$

where $\tilde{\boldsymbol{\Lambda}}^i$ is a diagonal matrix of eigenvalues for the kept normal modes of the i_{th} stage, and

$$\begin{aligned} \boldsymbol{\mu}^i_{\xi\xi} &= {\boldsymbol{\Pi}^i_{\sigma\xi}}^T \tilde{\boldsymbol{\mu}}^i_{\sigma\sigma} \boldsymbol{\Pi}^i_{\sigma\xi} \ , \quad \boldsymbol{\mu}^i_{\xi\Phi} = {\boldsymbol{\Pi}^i_{\sigma\xi}}^T \tilde{\boldsymbol{\mu}}^i_{\sigma\Phi} \\ \boldsymbol{\mu}^i_{\xi\upsilon} &= {\boldsymbol{\Pi}^i_{\sigma\xi}}^T \tilde{\boldsymbol{\mu}}_{\sigma\tau} \boldsymbol{\Pi}^i_{\tau\upsilon} \ , \quad \boldsymbol{\mu}^i_{\Phi\upsilon} = \tilde{\boldsymbol{\mu}}^i_{\Phi\tau} \boldsymbol{\Pi}^i_{\tau\upsilon} \\ \boldsymbol{\mu}^i_{\upsilon\upsilon} &= {\boldsymbol{\Pi}^i_{\tau\upsilon}}^T \tilde{\boldsymbol{\mu}}^i_{\tau\tau} \boldsymbol{\Pi}^i_{\tau\upsilon} \ , \quad \boldsymbol{\kappa}^i_{\xi\xi} = {\boldsymbol{\Pi}^i_{\sigma\xi}}^T \tilde{\boldsymbol{\kappa}}^i_{\sigma\sigma} \boldsymbol{\Pi}^i_{\sigma\xi} \\ \boldsymbol{\kappa}^i_{\xi\upsilon} &= {\boldsymbol{\Pi}^i_{\sigma\xi}}^T \tilde{\boldsymbol{\kappa}}^i_{\sigma\tau} \boldsymbol{\Pi}^i_{\tau\upsilon} \ , \quad \boldsymbol{\kappa}^i_{\upsilon\upsilon} = {\boldsymbol{\Pi}^i_{\tau\upsilon}}^T \tilde{\boldsymbol{\kappa}}^i_{\tau\tau} \boldsymbol{\Pi}^i_{\tau\upsilon} \end{aligned}$$

This synthesis process can be repeated for other stage-to-stage interfaces to generate a multi-stage CMS model for a rotor with an arbitrary number of stages.

3.4 Final Reduced-Order Model from Secondary Modal Analysis

The CMS model resulting from the synthesis process described above retains most of the DOF for the nodes at the stage-to-stage interfaces. For further reduction, secondary modal analysis can be performed on part or all of the matrices for the synthesized system [8]. In this study, the secondary modal analysis is performed on the entire multi-stage CMS model to yield a much more compact reduced-order model (ROM) in system modal coordinates:

$$\boldsymbol{q}^{rom} = \boldsymbol{q}^{syn}_{\Phi} \tag{12a}$$

$$\boldsymbol{\mu}^{rom} = \boldsymbol{\Phi}^{synT} \boldsymbol{\mu}^{syn} \boldsymbol{\Phi}^{syn} = \boldsymbol{I} \tag{12b}$$

$$\boldsymbol{\kappa}^{rom} = \boldsymbol{\Phi}^{synT} \boldsymbol{\kappa}^{syn} \boldsymbol{\Phi}^{syn} = \boldsymbol{\Lambda}^{syn}, \tag{12c}$$

where $\boldsymbol{\Phi}^{syn}$ and $\boldsymbol{\Lambda}^{syn}$ are the eigenvector matrix and the diagonal eigenvalue matrix for the kept modes from the secondary modal analysis, and $\boldsymbol{q}^{syn}_{\Phi}$ are generalized modal coordinates corresponding to the modes $\boldsymbol{\Phi}^{syn}$. Note that these multi-stage system modes may be selected for any frequency window of interest, just as in a traditional modal analysis.

4 NUMERICAL RESULTS FOR A TWO-STAGE ROTOR

In order to explore the vibration characteristics of a multi-stage rotor and to validate the new reduced-order modeling technique, a two-stage compressor rotor was examined. Fig. 6 shows a finite element model of the two-stage rotor that was used to obtain numerical results. This FE model is composed of standard linear brick elements, and the total number of DOF is 100,557. There are 27 blades in stage 1 and 35 blades in stage 2. As mentioned in the previous section, Fig. 7 illustrates the mismatch of the interface between these two stages. Finite element analysis of the full two-stage rotor shown in Fig. 6 was performed, with the stages connected using multi-point-constraints with linear interpolation, so that benchmark finite element results could be obtained for testing the accuracy of the ROM results. For the interfaces to omitted stages, the boundary DOF were held fixed in the axial direction only ("sliding" boundary conditions). The finite element software ANSYS [19] was used for this finite element analysis of the full two-stage rotor.

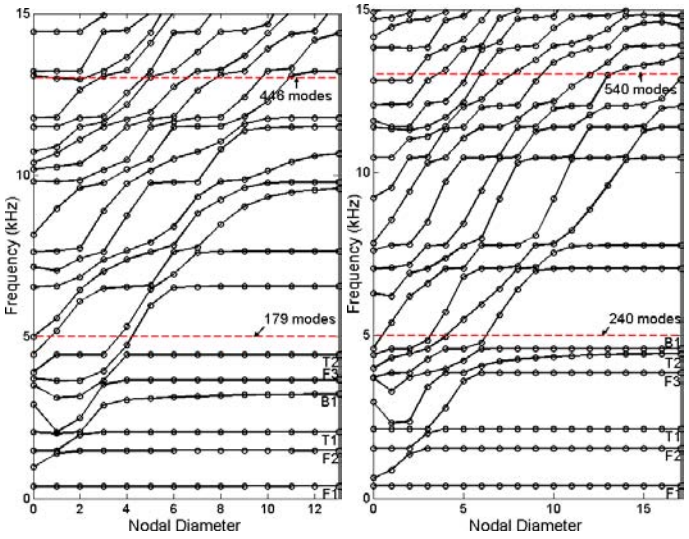

(a) STAGE 1 (b) STAGE 2

Figure 8. FIXED-INTERFACE NORMAL MODE FREQUENCIES

For the ROM calculation, component normal modes and constraint modes of individual stages were calculated using ANSYS cyclic symmetry routines. Fixed-interface normal mode frequencies for each stage are shown in Fig. 8. For this example model, the frequency range of interest is 0–5 kHz, which includes blade-dominated mode families for three flexural bending modes (F1, F2, F3), two torsion modes (T1, T2), and one edgewise bending mode (B1). Then MATLAB [20] was used to carry out the component synthesis and secondary modal analysis.

Figure 9(a) shows the natural frequency error of the synthesized model with component normal modes up to 13 kHz and various numbers of Fourier basis shapes used to describe the interface motion. As can be seen, the synthesized model with 19 Fourier basis shapes has maximum frequency error of 1.25%

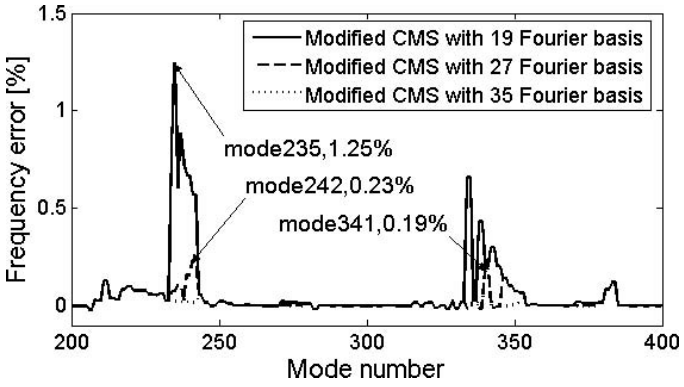

(a) WITH COMPONENT MODES UP TO 13 kHz

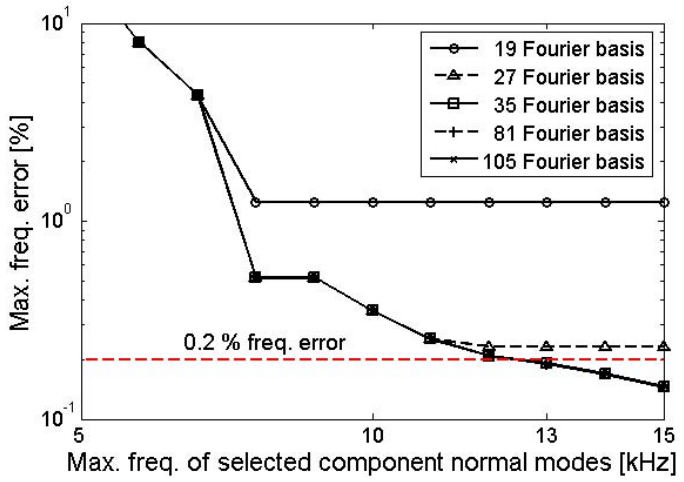

(b) MODAL CONVERGENCE

Figure 9. NATURAL FREQUENCY ERROR OF TWO-STAGE MODEL

at mode 235, and the model with 27 Fourier basis shapes has maximum frequency error of 0.23% at mode 242. These errors were caused by the lack of higher harmonic content for the retained Fourier shapes, and thus they can be reduced by increasing the number of harmonics. Note that the errors were reduced significantly when 35 Fourier basis shapes were retained. The maximum frequency error for this model is 0.19% at mode 341, which is mostly caused by the truncation of the component normal modes kept for the synthesized model.

As can be seen in Fig. 9(b), the natural frequencies for the synthesized ROM converge to those of the full FEM as the numbers of kept component normal modes and Fourier basis shapes are increased. For this numerical investigation, component modes in the frequency range up to 13 kHz were retained, and 35 Fourier basis shapes were kept, to achieve less than 0.2% frequency error. (Note that the number of Fourier basis shapes is same as the number of blades of stage 2, which has more blades than stage 1.) Using this selected basis, the synthesized model has 986 modal coordinates corresponding to 446 component normal modes of stage 1, 540 component normal modes of stage 2, and 315 interface shapes (35 Fourier basis shapes $\times$ 9 DOF on a fundamental radial segment), yielding a CMS model with a total of 1301 DOF.

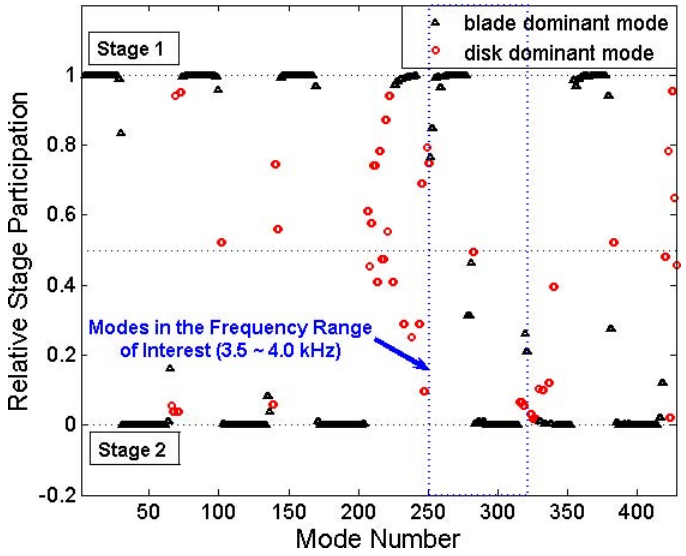

(a) FREQUENCY RANGE 0–5 kHz

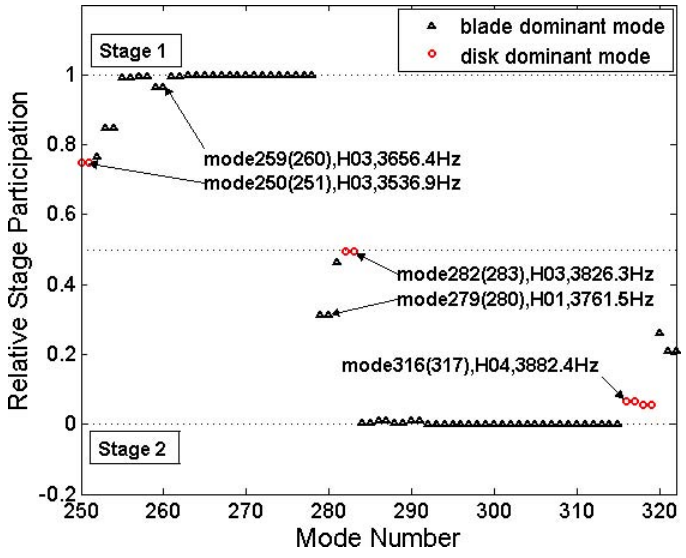

(b) FREQUENCY RANGE 3.5–4 kHz

Figure 10. RATIO OF STAGE 1 STRAIN ENERGY TO TOTAL MULTI-STAGE SYSTEM STRAIN ENERGY

Then a modal analysis was performed to retrieve multi-stage system modes, and each mode was characterized by the ratio of strain energy in stage 1 to the total strain energy of the

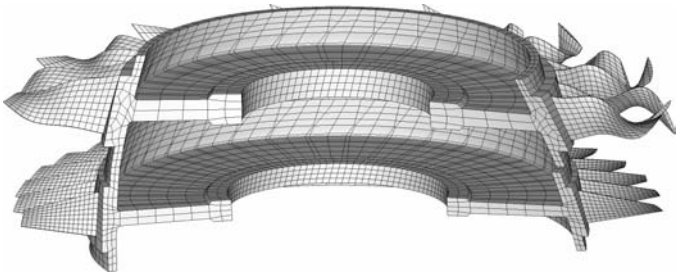

(a) WEAKLY COUPLED MODE (MODE 259)

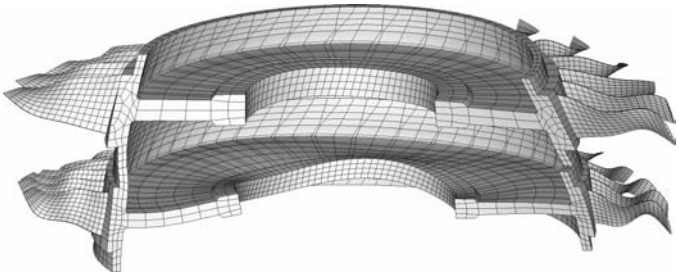

(b) STRONGLY COUPLED MODE (MODE 282)

Figure 11. MULTI-STAGE SYSTEM MODES

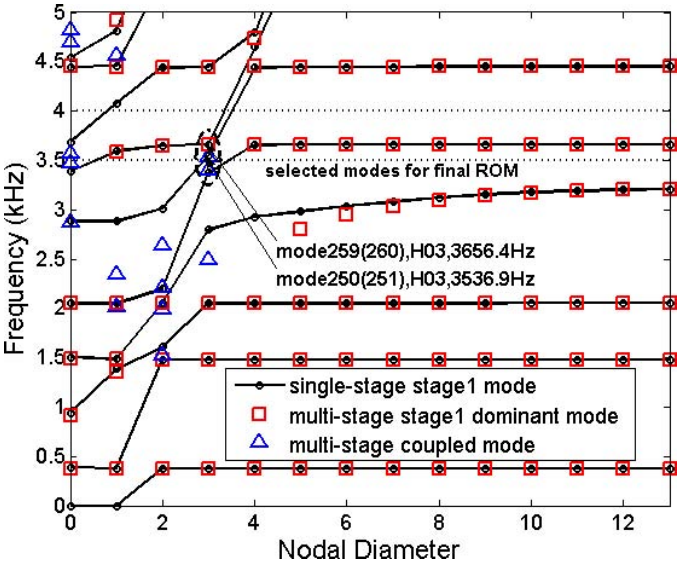

(a) STAGE 1 DOMINANT MODES

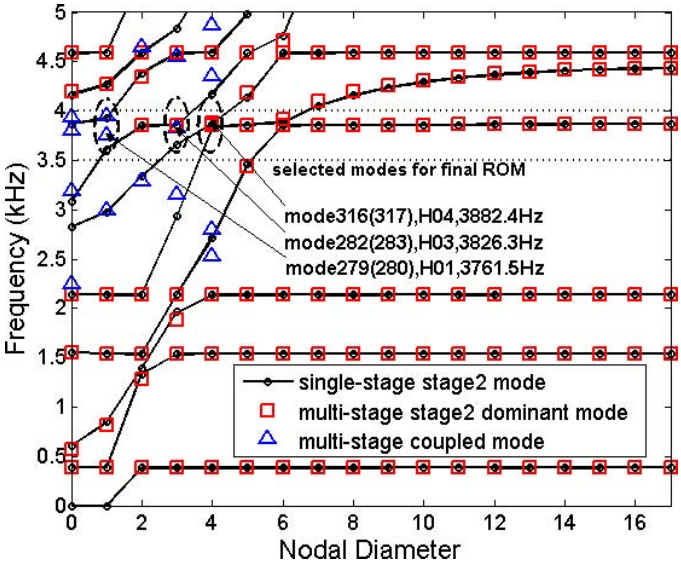

(b) STAGE 2 DOMINANT MODES

Figure 12. CLASSIFICATION OF MULTI-STAGE SYSTEM MODES AND COMPARISON WITH SINGLE-STAGE MODES

two-stage system. Figure 10 shows the relative stage participation for the individual modes of the two-stage rotor, as defined by this strain energy ratio. As can be seen, there exist many modes that show coupling among stages, which include both disk-dominated modes and blade-dominated modes. Modes 259 and 316 are weakly coupled between the two stages, and mode 259 is shown in Fig. 11(a). On the contrary, modes 250, 279, and 282 are strongly coupled across stages, and mode 282 is shown in Fig. 11(b).

Even though mistuning is not considered, the two-stage rotor is not a cyclic system. However, many modes that are largely confined to one of the stages resemble nodal diameter modes. Furthermore, for any mode, the motion can be decomposed into the circumferential harmonics to determine the dominant nodal diameter content. In this way, the modes from the multi-stage model can be classified according to stage participation and number of nodal diameters, and a plot of the number of nodal diameters versus natural frequencies can be obtained for the two-stage rotor and compared to those of the individual stages, as shown in Fig. 12. These plots help provide insight into the effects of the stage-to-stage coupling. As can be seen, modes 250 and 259 are located in a veering region for stage 1, and modes 279, 282, and 316 are located in a veering region for stage 2. In a veering region, the rotor vibration tends to feature a mix of disk and blade motion, and thus veerings are critical regions in that both the blade and disk dynamics must be well captured in order to predict the system vibration response. Therefore, for the final reduced-order model, 73 multi-stage modes in the frequency range 3.5–4.0 kHz were selected, which includes these veering regions. Table 1 shows the number of DOF for the initial finite element model, the intermediate CMS model, and the final reduced-order model.

For a forced response case, point forces were applied at the blade tips of stage 2, and both engine order 1 and 4 excitation

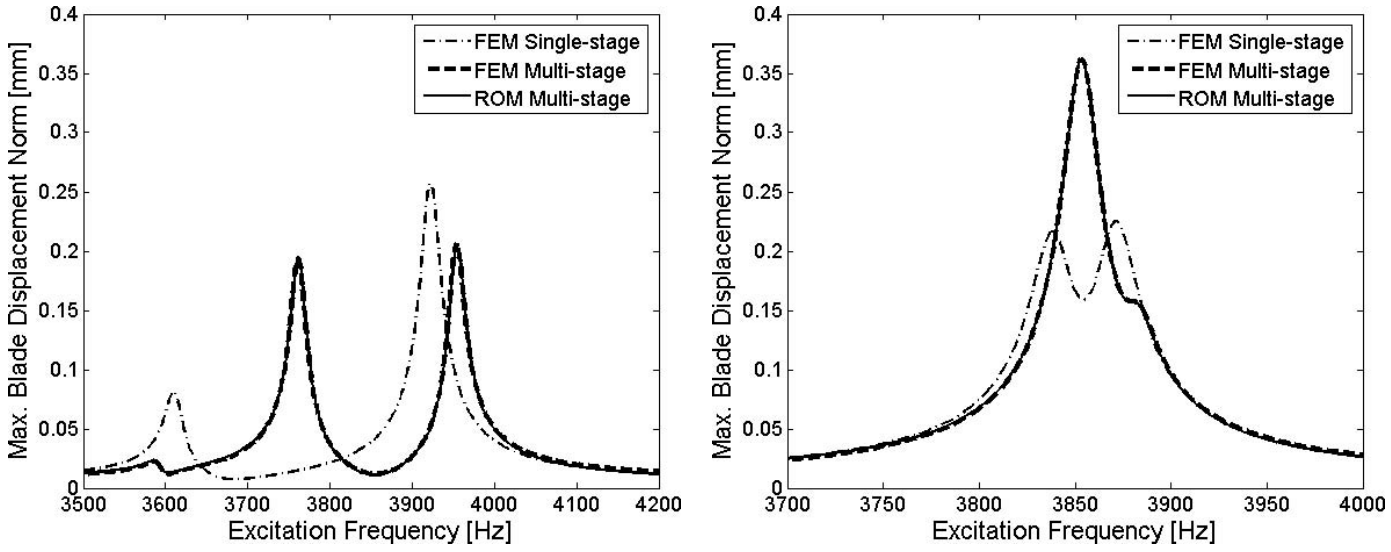

(a) ENGINE ORDER 1

(b) ENGINE ORDER 4

Figure 13. MULTI-STAGE FORCED RESPONSE

Table 1. NUMBER OF DOF IN THE TWO-STAGE ROTOR MODELS

Model	Stage 1	Stage 2	Interface	Total
Full FEM	42,282	57,330	945	100,557
CMS Model	446	540	315	1,301
ROM	-	-	-	73

cases were run. These engine orders correspond to the veering regions of interest. The maximum blade displacement norms for stage 2 of the two-stage ROM were compared to the results from the single-stage and two-stage FEMs. Figure 13 shows the forced response results. Note that there are significant differences between two-stage and single-stage FEM results, which indicates that a multi-stage model is needed to capture the effects of the stage-to-stage coupling on the vibration response of stage 2 in this region. In this regard, it is clear that the multi-stage modeling method introduced in this paper performed well, as the forced response results calculated with the 73-DOF multi-stage ROM show excellent agreement with the results from the full multi-stage FEM.

5 CONCLUSIONS

A reduced-order modeling method for multi-stage rotors was introduced, which is capable of handling the general case of different numbers of blades and finite element mesh mismatches between adjacent stages. The method is based on a framework of component mode synthesis, with each stage (bladed disk) treated as a separate component. Thus, each component structure has cyclic symmetry, and single-sector finite element models may be used to calculate the component normal modes and constraint modes in a highly efficient manner.

Synthesis at the interface between stages is achieved by projecting the constraint modes for each component onto a common basis of shapes that are harmonic in the circumferential direction. By neglecting higher harmonics, there is a one-to-one correspondence of retained shapes defining the interface motion for each component, which ensures displacement compatibility between stages. This obviates the need for manually applying multi-point constraints between stages, and it enables the systematic generation of a multi-stage CMS model based on a separate cyclic symmetry analysis of the single-sector finite element model for each stage of interest.

Further order reduction is achieved by performing a modal analysis on the CMS model, resulting in a highly compact reduced-order model in multi-stage system modal coordinates. For an example two-stage rotor, it was found that the reduced-order model was very accurate relative to the full finite element model.

For this initial study, the focus was on developing and validating the stage-to-stage synthesis and order reduction processes, and mistuning was not considered. However, it is believed that this new multi-stage modeling method can be combined with a recently developed mistuning projection technique [11] to handle the important case of mistuned multi-stage rotors. This will be explored in future research.

ACKNOWLEDGMENT

This work was performed under a Pratt & Whitney subcontract on a DARPA-funded Engine System Prognosis project, contract HR0011-04-C-0001. The support of Pratt & Whitney and DARPA is gratefully acknowledged.

REFERENCES

[1] Dye, R. C. F., and Henry, T. A., 1969. "Vibration Amplitudes of Compressor Blades Resulting From Scatter in Blade Natural Frequencies". *ASME Journal of Engineering for Power,* **91**(3), pp. 182–188.

[2] Ewins, D. J., 1969. "The Effects of Detuning Upon the Forced Vibrations of Bladed Disks". *Journal of Sound and Vibration,* **9**(1), pp. 65–79.

[3] Griffin, J. H., and Hoosac, T. M., 1984. "Model Development and Statistical Investigation of Turbine Blade Mistuning". *ASME Journal of Vibration, Acoustics, Stress, and Reliability in Design,* **106**(2), pp. 204–210.

[4] Wei, S. -T., and Pierre, C., 1988. "Localization Phenomena in Mistuned Assemblies with Cyclic Symmetry Part I: Free Vibrations". *ASME Journal of Vibration, Acoustics, Stress, and Reliability in Design,* **110**, pp. 429–438.

[5] Wei, S. -T., and Pierre, C., 1988. "Localization Phenomena in Mistuned Assemblies with Cyclic Symmetry Part II: Forced Vibrations". *ASME Journal of Vibration, Acoustics, Stress, and Reliability in Design,* **110**, pp. 439–449.

[6] Castanier, M. P., Ottarsson, G., and Pierre, C., 1997. "A Reduced Order Modeling Technique for Mistuned Bladed Disks". *ASME Journal of Vibration and Acoustics,* **119**(3), pp. 439–447.

[7] Bladh, R., Castanier, M. P., and Pierre, C., 1999. "Reduced order modeling and vibration analysis of mistuned bladed disk assemblies with shrouds". *ASME Journal of Engineering for Gas Turbines and Power,* **121**(3), pp. 515–522.

[8] Bladh, R., Castanier, M. P., and Pierre, C., 2001. "Component-Mode-Based Reduced Order Modeling Techniques for Mistuned Bladed Disks, Part I: Theoretical Models". *ASME Journal of Engineering for Gas Turbines and Power,* **123**, pp. 89–99.

[9] Bladh, R., Castanier, M. P., and Pierre, C., 2001. "Component-Mode-Based Reduced Order Modeling Techniques for Mistuned Bladed Disks, Part II: Application". *ASME Journal of Engineering for Gas Turbines and Power,* **123**, pp. 100–108.

[10] Moyroud, F., Fransson, T., Jacquet-Richardet, G., 2002. "A Comparison of Two Finite Element Reduction Techniques for Mistuned Bladed Disks". *Transactions of the ASME,* **124**, pp. 942–952.

[11] Lim, S., Bladh, R., Castanier, M. P., and Pierre, C., 2003. "A Compact, Generalized Component Mode Mistuning Representation for Modeling Bladed Disk Vibrations". In AIAA Paper 2003-1545, Proceedings of the 44th AIAA/ASME/ASCE/AMS Structures, Structural Dynamics, and Material Conference Norfolk, VA, Vol. 2, pp. 1359–1380.

[12] Yang, M. T., and Griffin, J. H., 2001. "A Reduced-Order Model of Mistuning Using a Subset of Nominal System Modes". *ASME Journal of Engineering for Gas Turbines and Power,* **123**(4), pp. 893–900.

[13] Petrov, E. P., Sanliturk, K. Y., and Ewins, D. J., 2002. "A New Method for Dynamic Analysis of Mistuned Bladed Disks Based on the Exact Relationship Between Tuned and Mistuned Systems". *ASME Journal of Engineering for Gas Turbines and Power,* **124**, pp. 586–597.

[14] Bladh, R., Castanier, M. P., and Pierre, C., 2003. "Effects of Multistage Coupling and Disk Flexibility on Mistuned Bladed Disk Dynamics". *ASME Journal of Engineering for Gas Turbines and Power,* **125**, pp. 121–130.

[15] Hurty, W. C., 1965. "Dynamic Analysis of Structural Systems Using Component Modes". *AIAA Journal,* **3**(4), pp. 678–685.

[16] Craig, R. R., Jr., and Bampton, M. C. C., 1968. "Coupling of Substructures for Dynamic Analyses". *AIAA Journal,* **6**(7), pp. 1313–1319.

[17] Craig, R. R., Jr., 1981. *Structural Dynamics: An Introduction to Computer Methods*. John Wiley & Sons, New York, ch. 19.

[18] Bladh, J. R., 2001. "Efficient Predictions of the Vibratory Response of Mistuned Bladed Disks by Reduced Order Modeling". PhD thesis, The University of Michigan, Ann Arbor.

[19] ANSYS, INC., 2004. *ANSYS Release 8.1 Documentation*. Pittsburgh, PA.

[20] MATHWORKS, INC., 2004. *MATLAB version 7.0 (R14)*. Natick, MA.